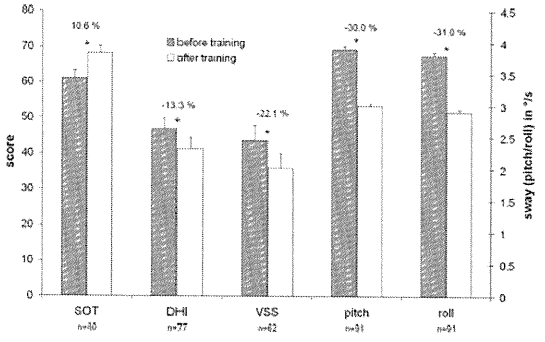

FIG. 2. Mean values (+ standard error of the mean [SEM]) and percentage changes of the SOT (BalanceMaster/Neurocom), the DHI, the VSS, and the body sway (pitch/roll) before and after a vibrotactile neurofeedback training in the treatment group. Numbers given below represent the number of patients included in the measurement. *Asterisks* indicate significant differences.

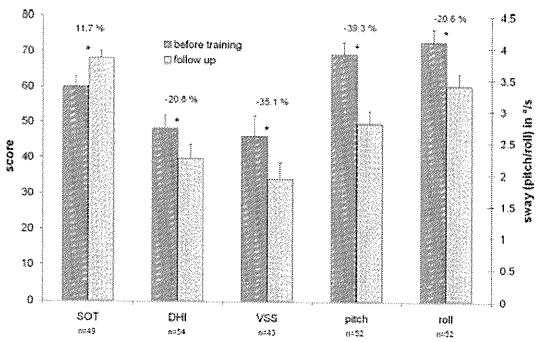

FIG. 3. Mean values (+SEM) and percentage changes of the SOT (BalanceMaster/Neurocom), the DHI, the VSS, and the body sway (pitch/roll) before a vibrotactile neurofeedback training and 3 months after the training in the treatment group. Numbers given below represent the number of patients included in the measurement. *Asterisks* indicate significant differences.

the probability of detecting a change, given that a change has occurred and effect size emphasizes the size of the change rather than confounding this with sample size. Both are very useful for the practical evaluation of the p value. The highest (best) value for the statistical power is 1. A sufficient effect size is higher than 0.5. The level of significance in all tests applied was $p < 0.05$.

A review board approved the study protocol. The patients gave their written, informed consent to participate in the study.

This study was carried out in accordance with the requirements of DIN EN ISO 14155-1/2.

RESULTS

Total Treatment and Placebo Group

The study was conducted from August 2009 until December 2010. No statistically significant differences could be determined with respect to age and sex between the treatment and placebo group (treatment/placebo: sex 42.8%/42.9% female, 57.2%/57.1% male; age 60.6 ± 13.3/61.3 ± 9.2).

The results of the primary end points before and immediately after the training were statistically significantly different in the treatment group (Fig. 2). The trunk sway decreased in the pitch direction by 30% (power, 1.00; effect size, 0.81) and 31% in roll direction (power, 0.99; effect size, 0.65).

The composite score of the SOT increased significantly (increase of stability) by 10.6% on average (power, 0.99; effect size, 0.64). This increase was mainly related to an improved performance in Tasks 5 and 6 of the SOT (Table 2).

The data of the secondary end points, the scores of the questionnaires DHI and VSS, were significantly reduced (reduced symptoms) after the training (power, 0.99; effect size, 0.48; and power, 0.99; effect size, 0.63, respectively). Significant differences also were found for all investigated parameters at the follow-up over time (Fig. 3), although only 60% of the initial patients attended the follow-up measures.

No statistically significant differences could be observed for trunk sway measures or in the SOT immediately after the training of the placebo group (Fig. 4) even if the SOT tasks were separately analyzed (Table 2). The same holds true for the secondary end points, the DHI, and the VSS (Fig. 4).

Treatment Subgroups

Analysis of Pathologic Conditions

The percentage of patients with a pathologic sway is shown for each condition of the SBDT in Figure 5. In all subgroups, the most frequent training tasks were on a foam support surface. There seems to be a trend for a lower occurrence of pathologic sway in walking conditions for patients with otolith disorders. Patients of the PD, MVCS, and P subgroup showed a pathologic sway also frequently in walking tasks.

TABLE 2. *Results of the Sensory Organization Test on the BalanceMaster (Neurocom) for tasks 1 to 4 and 5 to 6*

	Treatment group			Placebo group		
Task	Before training	After training	p value	Before training	After training	p value
SOT 1 4	80.9 + 1.6	82.5 + 1.5	0.074	74.5 + 7.0	78.7 + 5.4	0.103
SOT 5 6	40.9 + 3.2	54.0 + 3.1	0.001*	47.2 + 11.4	54.0 + 8.4	0.475

Data shown are for the treatment and placebo groups. Asterisks indicate significant differences between values before and after the training.

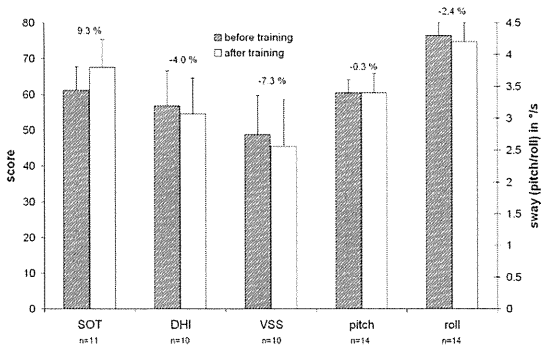

FIG. 4. Mean values (±SEM) and percentage changes of the SOT (BalanceMaster/Neurocom), the DHI, the VSS, and the body sway (pitch/roll) before and after a vibrotactile neurofeedback training in the placebo group. Numbers given below represent the number of patients included in the measurement. *Asterisks* indicate significant differences.

Effect of Training on Trunk Sway

The trunk sway in pitch direction was decreased significantly (Fig. 6) in all subgroups (SCC: power, 0.98; effect size, 0.77; O: power, 0.83; effect size, 0.59; AN: power, 0.76; effect size, 0.81; MVCS: power, 0.58; effect size, 0.63; P: power, 0.98; effect size, 1.13; PD: power, 0.98; effect size, 1.28). Figure 7 shows the mean group values of the trunk sway in roll direction before and after the training. The trunk sway in roll direction was significantly decreased after the training in all subgroups with the exception of the MVCS patients (SCC: power, 0.91; effect size, 0.61; O: power, 0.63; effect size, 0.45; AN: power, 0.81; effect size, 0.86; P: power, 0.75; effect size, 0.68; and PD: power, 0.99; effect size, 1.38).

Effect of Training on SOT Composite Score

A significant increase of the SOT composite score (Conditions 1–6) could be observed in the SCC (power, 0.95; effect size, 0.73), O (power, 0.7; effect size, 0.55), P (power, 0.84; effect size, 0.77), and PD (power, 0.84; effect size, 0.91) subgroups (Fig. 8). Patients of the AN and MVCS subgroups increased their stability on the platform not statistically significantly on average (Fig. 8).

Effect of Training on DHI Score

The DHI score, as one of the secondary end points, showed significant differences only in the SCC and PD groups (Fig. 9) with a statistical power of 0.7 (effect size, 0.55) and 0.95 (effect size, 1.15), respectively.

Only a trend for a reduced DHI score was visible for the AN, MVCS, and P group.

Effect of Training on VSS Score

The other secondary end point, the VSS scores, was significantly reduced in the SCC and O groups (Fig. 10). The statistical power was 0.94 (effect size, 0.9) for the SCC and 0.93 (effect size, 0.84) for the O group. A trend for a reduction of the mean VSS score was observed for all other investigated subgroups. Patients of the PD group were not asked to fill in the VSS questionnaire.

DISCUSSION

The present results indicate that a specific vibrotactile neurofeedback rehabilitation program, which is "tailored" to meet the needs of the individual balance deficit, can significantly improve the postural control in stance and gait situations. This could be demonstrated by the significant reduction of body sway in pitch and roll directions during everyday-life test conditions and the significant increase of stability (SOT composite score) in different sensorimotor stance conditions (force plate measurements). The performance on the SOT improved especially in the more vestibular related Tasks 5 and 6. This finding indicates the specific effect of the training on vestibular rehabilitation.

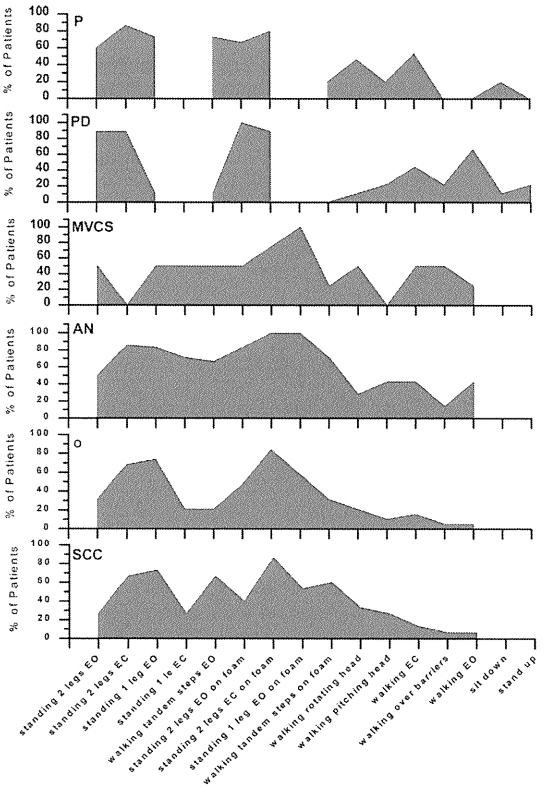

FIG. 5. Percentage of patients with a pathologic body sway during the conditions of the Standard Balance Deficit Test. Patients were analyzed within the following subgroups: P, presbyvertigo; PD, Parkinson's disease; SCC, semicircular canal paresis; O, otolith disorder; AN, removal of an acoustic neuroma; MVCS, micro(neuro) vascular compression syndrome. P and PD patients performed the geriatric Standard Balance Deficit Test where the "standing on 1 leg EC" and the "standing on 1 leg EO on foam" tasks were replaced by "sit down" and "stand up." All other subgroups performed the Standard Balance Deficit Test, which not includes the "sit down" and "stand up" tasks.

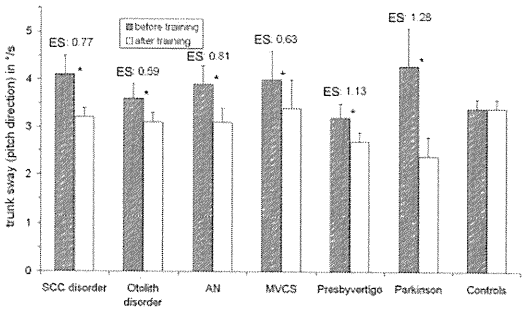

FIG. 6. Mean values (+SEM) of the body sway in pitch direction before and after a vibrotactile neurofeedback training in treatment subgroups. *Asterisks* indicate significant differences. ES indicates effect size.

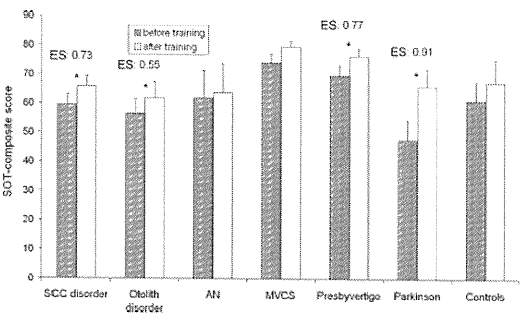

FIG. 8. Mean values (+SEM) of the SOT (BalanceMaster/ Neurocom) before and after a vibrotactile neurofeedback training in treatment subgroups. *Asterisks* indicate significant differences.

The reliability and clinical relevance of the results could be proven by a power value of approximately 1 and an effect size of more than 0.6. Moreover, the improvement was present only in patients of the feedback-training group compared with the controls. The finding that training with a sham device had no influence on body sway is in contrast to earlier studies, which investigated the effect of physical exercises in healthy subjects (19). It could be possible that the training sessions of the present study were too short to induce such learning effects by repetition. Each of the exercise was repeated only 5 times for 20 seconds in the daily sessions. This is in line with previous studies of short training sessions in everyday-life conditions, which had no significant effect on the postural stability without applying an additional feedback signal during the training (15).

The underlying neural mechanisms for the training effect might involve operant learning (20) and the multisensory convergence of enhanced processing of different sensory modalities (21). When the patients' reactions to the vibrotactile feedback signal result in a reduction of trunk sway, they have to memorize the activation template of the proprioceptive system for this situation. Without vibrotactile feedback, the activation template of the proprioceptive system has to be maintained at the same level to ensure postural control. Those neural structures encoding more than one sensory modality are best suited for spatial information processing (22). In primates, the parietal cortex seems to play a key role in this procedure (23).

However, each learning process should be followed by unlearning. The improvements induced by the vibrotactile training in the present study also were observed after a 3-months' follow-up. Although, all patients were invited to the follow-up measures, only 60% attended. One reason or implication is that 40% of the patients had no further interest in the study because his/her vestibular problems disappeared after the training. It is a very frequent effect in clinical practice. If this holds true, only patients with consisting vestibular problems were included in the follow-up measures. The effect of the training is possibly much higher than reported after 3 months.

The observed long-term effect is in line with earlier studies in chronic unilateral vestibular hypofunction or in PD where only a small number of supervised sessions were sufficiently enough to obtain a long-lasting improvement of postural stability (3,6).

The vibrotactile neurofeedback signal seems to be a very effective stimulus for vestibular rehabilitation

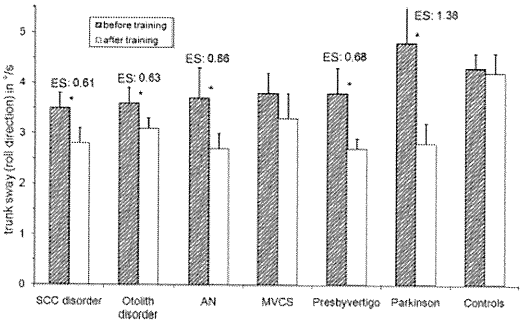

FIG. 7. Mean values (+SEM) of the body sway in roll direction before and after a vibrotactile neurofeedback training in treatment subgroups. *Asterisks* indicate significant differences.

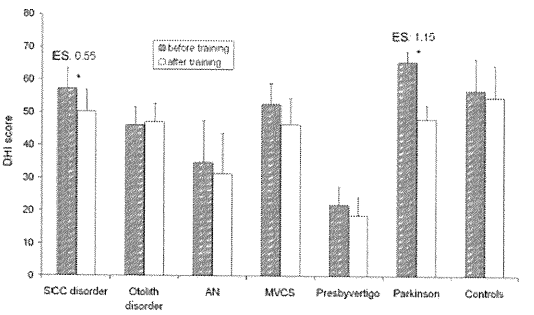

FIG. 9. Mean values (+SEM) of the DHI before and after a vibrotactile neurofeedback training in treatment subgroups. *Asterisks* indicate significant differences.

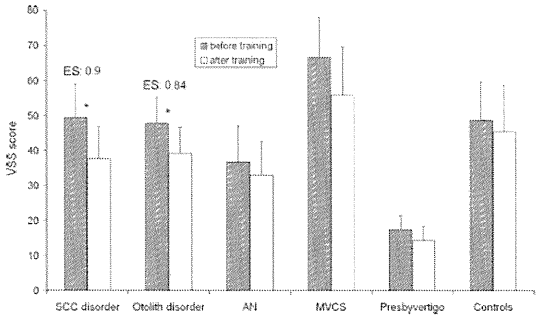

FIG. 10. Mean values (+SEM) of the VSS before and after a vibrotactile neurofeedback training in treatment subgroups. *Asterisks* indicate significant differences.

because its perception by the patients during the training is very intuitive. Furthermore, no important, other sensory input channels (e.g., auditory, visual) are impaired by the vibrotactile signal so that no sensory conflict occur, and the signal processing is not influenced by simultaneous vestibular stimulation (as known for auditory signals [24]). However, a vibration-induced illusion of movement was described in previous studies (25), but the strength and duration of vibration, which is necessary to induce such effects, cannot be provided by the vibrotactile feedback system used in the present study (Vertiguard). The vibrotactile stimulation applied with the Vertiguard was very short (approximately 1 s) and only slightly above the perception threshold. If there is nevertheless an influence of the vibration itself on some trunk muscle reflexes, these reflexes would act in the same direction as intended by the training (move to the opposite site) and would therefore support the intended application of the device.

The subjective parameters—such as DHI and VSS scores—were significantly reduced with a high statistical power and effect size in the treatment group only. The controls showed a small, but not significant, reduction of these symptom-related scores. This is somewhat surprising because the dissociation between self-perception and actual vestibular handicap was reported previously (26,27).

Treatment Subgroups

The broad distribution of training tasks within each subgroup indicates the need of an individualized training program, which is based on a standardized body sway analysis. This holds true even if some tasks were more frequent pathologic in 1 subgroup than in another subgroup. The most frequent pathologic tasks were quite similar in all subgroups. Therefore, it seems not to be possible to develop a specific training procedure for specific pathologies with this method.

The analysis of disease-related subgroups within the total treatment sample showed different training effects in some of the investigated parameters. Even if body sway during everyday life conditions could be significantly reduced in all subgroups, patients with PD or presbyvertigo showed the highest absolute reduction. The high efficacy of the neurofeedback training in these subgroups is possibly related to the fact that central compensation could occur without pathologic inputs of the peripheral vestibular organs. This hypothesis is supported by the present results of the SOT on the BalanceMaster (stance conditions). Patients with an irregular input of peripheral vestibular afferents (e.g., MVCS subgroup) showed a nonsignificant improvement. In these patients, the peripheral vestibular afferents depend largely on variable parameters such as blood pressure and pulse rate, which in turn trigger the functional status of the corresponding artery—that is, the anterior inferior cerebellar artery.

The results of the investigated subjective parameters differed between the subgroups. Only patients of the SCC group showed a significantly decreased DHI and VSS score after the training. The VSS scores, but not the DHI scores, were decreased in patients with an otolith disorder. This is in accordance with previous results of auditory neurofeedback training in those patients (15).

The highest reduction of symptom scores, combined with the largest statistical power and effect size, was observed in the PD group. However, the mean values of these patients before and after the training was the highest of all investigated subgroups. The subjective parameters (VSS/DHI) of the P group were not significantly reduced even if the objective decrease of body sway was statistically significant. On the one hand, this could rely on a correlation between the absolute changes of the scores and the low pretraining values. The overall extent of reductions in DHI scores was, for example, 11.9% for the SCC group (statistically significant) and 14.8% for the P group (not statistically significant). On the other hand, the dissociation between self-perception and postural handicap holds possibly particularly true for the elderly (26,27).

In essence, the vibrotactile neurofeedback training applied in the present study is a highly efficient method for the reduction of body sway in different balance disorders. Because the rehabilitation program is easy to perform, not exhausting and time saving, elderly patients and those with serious, long-lasting balance problems also can participate successfully.

REFERENCES

1. Curthoys IS. Vestibular compensation and substitution. *Curr Op Neurol* 2000;13:27 30.
2. Hansson EE, Mansson NO, Hakansson A. Effects of specific rehabilitation for dizziness among patients in primary health care. A randomized controlled trial. *Clin Rehab* 2004;18:558 65.
3. Rossi-Izquierdo M, Soto-Varela A, Santos-Pérez S, Sesar-Ignacio A, Labella Caballero T. Vestibular rehabilitation with computerized dynamic posturography in patients with Parkinson's disease: improving balance impairment. *Disabil Rehabil* 2009;31:1907 16.
4. Asai M, Watanabe Y, Shimizu K. Effects of vestibular rehabilitation on postural control. *Acta Otolaryngol Suppl* 1997;528:116 20.
5. Topuz O, Topuz B, Ardic FN, Sarhus M, Ogmen G, Ardic F. Efficacy of vestibular rehabilitation on chronic unilateral vestibular dysfunction. *Clin Rehab* 2004;18:76 83.

6. McGibbon CA, Wayne PM, Scarborough DM, Parker SW. Tai Chi and vestibular rehabilitation effects on gaze and whole-body stability. *J Vest Res* 2004;14:467 78.
7. Pavlou M, Lingeswaran A, Davies RA, Gresty MA, Bronstein AM. Simulator based rehabilitation in refractory dizziness. *J Neurol* 2004;251:983 95.
8. Viirre E, Sitarz R. Vestibular rehabilitation using visual displays: preliminary study. *Laryngoscope* 2002;112:500 3.
9. Danilov YP, Tyler ME, Skinner KL, Hogle RA, Bach-y-Rita P. Efficacy of electrotactile vestibular substitution in patients with peripheral and central vestibular loss. *J Vestib Res* 2007;17:119 30.
10. Barros CG, Bittar RS, Danilov Y. Effects of electrotactile vestibular substitution on rehabilitation of patients with bilateral vestibular loss. *Neurosci Lett* 2010;476:123 6.
11. Kentala E, Vivas J, Wall C 3rd. Reduction of postural sway by use of vibrotactile balance prosthesis in subjects with vestibular deficits. *Ann Otol Rhinol Laryngol* 2003;112:404 9.
12. Wall C 3rd. Application of vibrotactile feedback of body motion to improve rehabilitation in individuals with imbalance. *J Neurol Phys Ther* 2010;34:98 104.
13. Dozza M, Horak FB, Chiari L. Auditory biofeedback substitutes for loss of sensory information in maintaining stance. *Exp Brain Res* 2007;178:37 48.
14. Hegemann J, Honegger F, Kupper M, Allum JHJ. The balance control of bilateral peripheral vestibular loss subjects and its improvement with auditory prosthetic feedback. *J Vest Res* 2005;15:1 8.
15. Basta D, Singbartl F, Todt I, Clarke A, Ernst A. Vestibular rehabilitation by auditory feedback in otolith disorders. *Gait Posture* 2008;28:397 404.
16. Faul F, Erdfelder E, Lang AG, Buchner A. G*Power 3: A flexible statistical power analysis program for the social, behavioral, and biomedical sciences. *Behav Res Methods* 2007;39:175 91.
17. Jacobson GP, Newman CW. The development of the dizziness handicap inventory (DHI). *Arch Otolaryngol Head Neck Surg* 1990; 116:424 7.
18. Tschan R, Wiltink J, Best C, et al. Validation of the German version of the Vertigo Symptom Scale (VSS) in patients with organic or somatoform dizziness and healthy controls. *J Neurol* 2008;255: 1168 75.
19. Brandt T, Krafczyk S, Malsbenden I. Postural imbalance with head extension: improvement by training as a model for ataxia therapy. *Ann NY Acad Sci* 1981;34:636 49.
20. Taub E, Crago JE, Burgio LD, et al. An operant approach to rehabilitation medicine: overcoming learned non-use by shaping. *J Exp Anal Behav* 1994;61:281 93.
21. Foxe JJ, Schroeder CE. The case for feedforward multisensory convergence during early cortical processing. *Neuroreport* 2005; 16:419 23.
22. Schlack A, Sterbing-D'Angelo SJ, Hartung K, Hoffmann KP, Bremmer F. Multisensory space representations in the macaque ventral intraparietal area. *J Neurosci* 2005;25:4616 25.
23. Bremmer F, Schlack A, Duhamel JR, Graf W, Fink GR. Space coding in primate posterior parietal cortex. *Neuroimage* 2001;14: 46 51.
24. Probst T, Wist ER. Impairment of auditory processing by simultaneous vestibular stimulation: psychophysical and electrophysiological data. *Behav Brain Res* 1990;41:1 9.
25. Verschueren SM, Swinnen SP, Desloovere K, Duysens J. Vibration-induced changes in EMG during human locomotion. *J Neurophysiol* 2003;89:1299 307.
26. Perez N, Martin E, Garcia-Tapia R. Dizziness: relating the severity of vertigo to the degree of handicap by measuring vestibular impairment. *Otolaryngol Head Neck Surg* 2003;128:372 81.
27. Whitney SL, Wrisley DM, Brown KE, Furman JM. Is perception of handicap related to functional performance in persons with vestibular dysfunction? *Otol Neurotol* 2004;25:139 43.

ELSEVIER

Auris Nasus Larynx 39 (2012) 208–211

AURIS NASUS LARYNX
INTERNATIONAL JOURNAL OF ORL & HNS

www.elsevier.com/locate/anl

A new device for delivering drugs into the inner ear: Otoendoscope with microcatheter

Sho Kanzaki *, Hideyuki Saito, Yasuhiro Inoue, Kaoru Ogawa

Department of Otolaryngology, Head and Neck Surgery, Keio University, School of Medicine, 35 Shinanomachi, Shinjuku, Tokyo 160-8582, Japan

Received 19 December 2010; accepted 22 April 2011
Available online 20 May 2011

Abstract

Objectives: Intratympanic injection (ITI) of drugs into the inner ear is an attractive way to deliver therapy. However, if the round window membrane (RWM) cannot be visualized, adhesions need to be removed first before ITI can be performed. We developed and tested a novel otoendoscopy device that allows visualization of the RWM for the purpose of ITI.
Methods: Our otoendoscope consists of a catheter channel for delivering drugs and a suction channel.
Results: The novel otoendoscope for inner ear drug delivery has a fine needle with catheter, which can be used to remove or perforate round window niche (RWN) mucosal adhesions. The elliptical shape of the otoendoscope effectively captures the field in the light-guided area, resulting in bright images.
Conclusions: Our otoendoscope can be used to apply drugs directly onto the surface of the RWM and to verify the correct placement of an inner ear drug delivery system, ensuring that it is safely in place.

Keywords: Inner ear; Round window membrane; Otoendoscope; Catheter; Drug delivery system

1. Introduction

The intratympanic injection (ITI) of drugs into the inner ear is a very attractive way for delivering therapy in Meniere's disease and idiopathic sensorineural hearing loss [1]. Delivering steroids by ITI is more efficient than by systemic injections. Trials have demonstrated that ITI is effective and decreases chances of side effects related to systemic steroid injections [1,2]. ITI, however, is a blind procedure. When the round window niche (RWN) is covered with fibrous or connective tissue, which occurs in about 10–30% of cases [1,3,4], it is impossible for drugs injected by ITI to reach the perilymph of the scala tympani via the round window membrane (RWM).

Therefore, if the RWM cannot be visualized, adhesions covering the RWM should be removed first through otoendoscopy before drugs are delivered [1]. Anatomic barriers to the RWM may be a significant cause of ITI failure [5]. Although drugs have been delivered successfully into the inner ear with the aid of microcatheters [6] or otoendoscopes [7] employing a working channel for drug injection, a separate instrument is needed to remove adhesions overlying the RWM. To address this issue, we developed a new otoendoscopy device that allows visualization of the RWM, removal of adhesions, and drug delivery.

2. Materials and methods

We developed an otoendoscope that consists of a fiber optic lens (0.6 mm) for viewing and two working channels (1.0 mm and 0.3 mm, respectively); a catheter channel for delivering drugs; and a suction channel for removing adhesions (Machida Corporation, Tokyo, Japan). The working length is 50 mm. The diameter of this device is

* Corresponding author. Tel.: +81 3 5363 3827; fax: +81 3 3353 1261.
E-mail address: skan@a7.keio.jp (S. Kanzaki).

0385-8146/$ – see front matter © 2011 Elsevier Ireland Ltd. All rights reserved.
doi:10.1016/j.anl.2011.04.006

only 2.4 mm × 1.4 mm, which is small enough for use in the inner ear and for approaching the small space around the RWN. The small diameter of such devices, however, exposes them to four potential problems—(1) low-quality images, (2) increased chance of clogging the channel with drug solution, (3) increased effort required to clean the channel, and (4) increased fragility—all of which we took into account during the development of our improved otoendoscope.

The otoendoscope system for inner ear drug delivery has the following features:

1. A 30-gauge needle attached to a catheter to remove or perforate RWN mucosal adhesions and to inject drugs (Fig. 1).
2. A catheter threaded inside the channel to deliver drug solutions so liquids never directly contact the working channel, preventing channel clogging.
3. An elliptical shape that enables our otoendoscopy device to more effectively capture the field in the light-guided area than prototype otoendoscopes, resulting in brighter and higher-quality images.

This modified otoendoscope has a similar bore as previous ones, but it is less fragile and less troublesome to use. We tested a conventional otoendoscope, a prototype otoendoscope, and the newly developed otoendoscope on cadaver temporal bones. Prior to using the drug delivery device, under otoendoscopy conventional myringotomy was performed with a small blade (2 mm) at the junction between the posteroinferior quadrants, and then the otoendoscope combined with a catheter was inserted into the inner ear.

All research was conducted with the approval of the Keio University Hospital Institutional Review Board and in accordance with the Helsinki Declaration. The novel otoendoscope inner ear drug delivery device is currently being developed for clinical use.

3. Results

We observed complete obstruction of the RWN in 2 of 5 cadaver temporal bones (Table 1). We also compared our otoendoscope with prototype (Machida Corporation, Tokyo Japan) or conventional otoendoscopes (Olympus Corporation Tokyo, Japan). After performing myringotomy, we used the three different types of otoendoscopes to view the RWM and found that our novel otoendoscope produced good-quality images of the RWM (Fig. 2A). However, because the lens contained within our otoendoscope is only 0.6 mm in diameter, image resolution was not as high-quality as that of the conventional otoendoscope we tested. Thus, the lens requires additional refinement. Although 30°-angled otoendoscopy is typically used to view the RWN, straight (0°) otoendoscopy

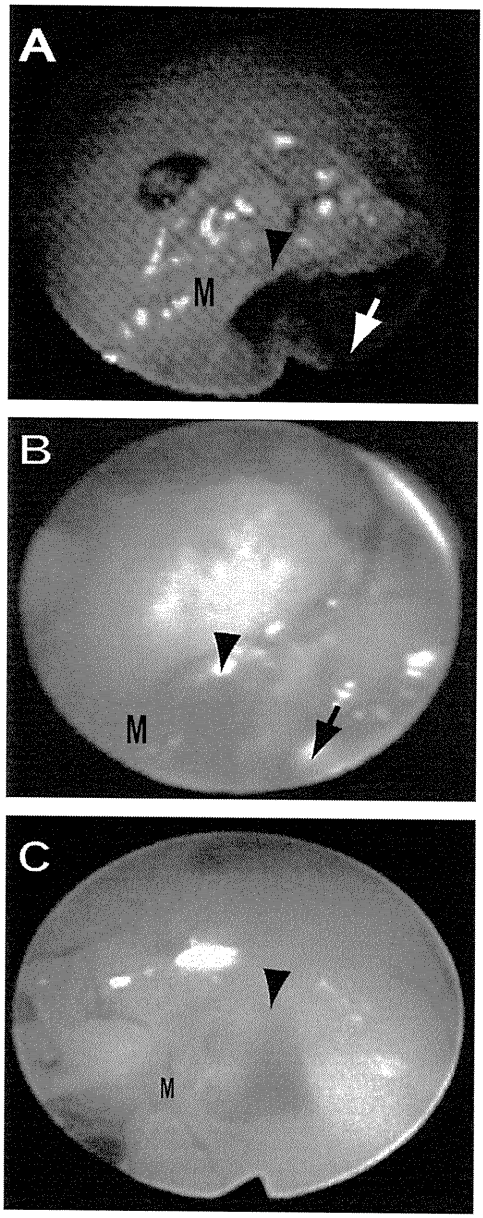

Fig. 1. Novel otoendoscope developed in our clinic. (A) Frontal view of the otoendoscope showing the lens (L) and two channels (W, working channel; *, suction channel). (B) Side view of the otoendoscope with catheter and needle. Scale bar: 5 cm. (C) High magnification view of the tip of the otoendoscope (E) showing the catheter (Ca) and needle (N). A catheter for angiography is also available for this scope. For inner ear procedures, a 30-gauge needle (*) is inserted into the tip of the catheter.

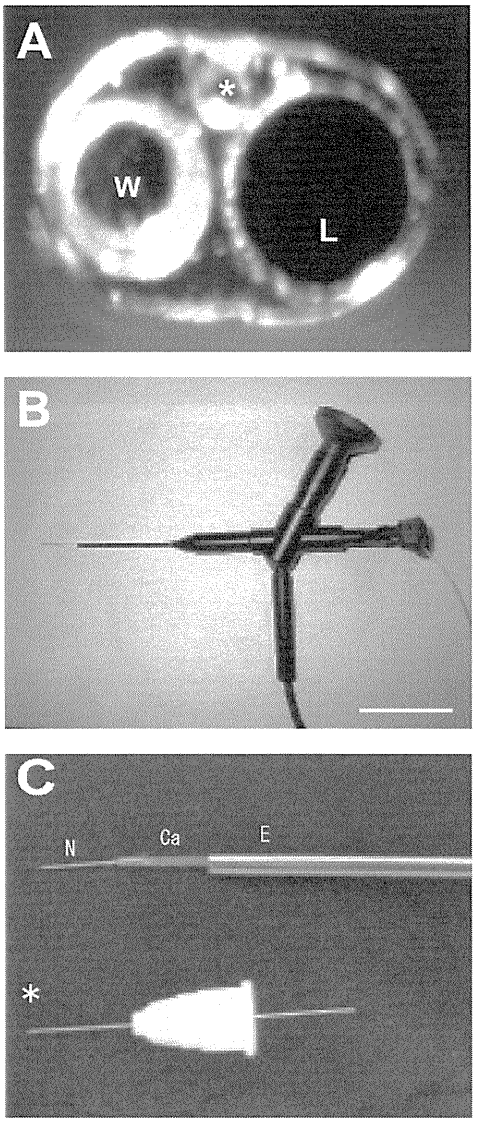

Fig. 2. Round window membrane (RWM indicated by "M" and arrowheads) images as visualized through different otoendoscopes. RWM images captured with the novel otoendoscope (A), a prototype otoendoscope (B), and a 30-angled (1.9 mm; Olympus) conventional otoendoscope (C). The image shown in panel C was especially of high quality. (A and B) Using a needle, we opened up the connective tissue overlying the RWN and injected a solution onto the RWM (M). The needles are indicated by arrows.

can also capture images of the RWM (Fig. 2). Because 0°-angled otoendoscopes are easier to handle, it may be easier to view RWM images through 0°-angled otoendoscopy than through 30°-angled otoendoscopy.

Table 1
RW obstruction of cadaver.

Case (age, sex)	Cadaver condition	RW obstruction
Unknown, F	Fixed	+
Unknown, F	Fixed	−
90 y/o, F	Unfixed	+
94 y/o, F	Unfixed	+/−
92 y/o, F	Unfixed	−

RWM obstruction +: present, +/−: partial present, −: not present.

Table 2
Comparison of different otoendoscopes.

	Results of comparison
Observation of RWM	C > N = P
Treatment of adhesions	N = C > P
Otoendoscope diameter (mm)	N(1.5) > C(1.9) > P(2.4)

C, conventional otoendoscope; N, novel otoendoscope with catheter; P, prototype otoendoscope with catheter.

4. Discussion

Our otoendoscope represents a new concept in treating and diagnosing inner ear-associated hearing loss. If ITI is unsuccessful, the RWM should be examined. This can be carried out conveniently with our otoendoscope. Additionally, our otoendoscope can be used also for diagnosing perilymphatic fistulas and for providing related therapy.

We compared the advantages and disadvantages of the novel otoendoscope, a prototype otoendoscope, and a conventional otoendoscope (Table 2). Although our otoendoscope is smaller than other types of otoendoscopes, it still captures an adequate image of the RWN. Moreover, our otoendoscope combined with a catheter can be used to evaluate the RWN before a local drug delivery system is put into place; to apply drugs directly onto the surface of the RWM; and to verify the correct placement of an inner ear drug delivery system, ensuring that it is safely in place.

Acknowledgements

We thank Mr. Ishikawa and his colleagues at Machida Corporation for helping develop the otoendoscope. This work was supported by grants from the Ministry of Health, Labor, and Welfare in Japan (H16-008 K.O. and S.K.), and Ministry of culture, sports, science and technology in Japan (20390444 K.O., R.T. and S.K.).

References

[1] Silverstein H, Choo D, Rosenberg SI, Kuhn J, Seidman M, Stein I, et al. Intratympanic steroid treatment of inner ear disease and tinnitus (preliminary report). Ear Nose Throat J 1996;75:468–71.

[2] Xenellis J, Papadimitriou N, Nikolopoulos T, Maragoudakis P, Segas J, Tzagaroulakis A, et al. Intratympanic steroid treatment in idiopathic sudden sensorineural hearing loss: a control study. Otolaryngol Head Neck Surg 2006;134:940–5.
[3] Sahni RS, Paparella MM, Schachern PA, Goycoolea MV, Le CT. Thickness of the human round window membrane in different forms of otitis media. Arch Otolaryngol Head Neck Surg 1987;113:630–4.
[4] Alzamil KS, Linthicum Jr FH. Extraneous round window membranes and plugs: possible effect on intratympanic therapy. Ann Otol Rhinol Laryngol 2000;109:30–2.
[5] Crane BT, Minor LB, Della Santina CC, Carey JP. Middle ear exploration in patients with Meniere's disease who have failed outpatient intratympanic gentamicin therapy. Otol Neurotol 2009;30:619–24.
[6] Plontke SK, Zimmermann R, Zenner HP, Lowenheim H. Technical note on microcatheter implantation for local inner ear drug delivery: surgical technique and safety aspects. Otol Neurotol 2006;27:912–7.
[7] Plontke SK, Plinkert PK, Plinkert B, Koitschev A, Zenner HP, Lowenheim H, et al. Transtympanic endoscopy for drug delivery to the inner ear using a new microendoscope. Adv Otorhinolaryngol 2002;59:149–155.

Neurochem Res (2011) 36:1261–1269
DOI 10.1007/s11064-011-0416-3

ORIGINAL PAPER

Expression and Function of Sox21 During Mouse Cochlea Development

Makoto Hosoya · Masato Fujioka · Satoru Matsuda · Hiroyuki Ohba · Shinsuke Shibata · Fumiko Nakagawa · Takahisa Watabe · Ken-ichiro Wakabayashi · Yumiko Saga · Kaoru Ogawa · Hirotaka James Okano · Hideyuki Okano

Accepted: 21 January 2011 / Published online: 3 February 2011

Abstract The development of the inner ear is an orchestrated process of morphogenesis with spatiotemporally controlled generations of individual cell types. Recent studies have revealed that the Sox gene family, a family of evolutionarily conserved HMG-type transcriptional factors, is differentially expressed in each cell type of the mammalian inner ear and plays critical roles in cell-fate determination during development. In this study, we examined the expression pattern of Sox21 in the developing and adult murine cochlea. Sox21 was expressed throughout the sensory epithelium in the early otocyst stage but became restricted to supporting cells during adulthood. Interestingly, the expression in adults was restricted to the inner phalangeal, inner border, and Deiters' cells: all of these cells are in direct contact with hair cells. Evaluations of the auditory brainstem-response revealed that $Sox21^{-/-}$ mice suffered mild hearing impairments, with an increase in hair cells that miss their appropriate planar cell polarity. Taken together with the previously reported critical roles of SoxB1 families in the morphogenesis of inner ear sensory and neuronal cells, our results suggest that Sox21, a counteracting partner of the SoxB1 family, controls fine-tuned cell fate decisions. Also, the characteristic expression pattern may be useful for labelling a particular subset of supporting cells.

Keywords Inner ear · Cochlea · Development · Sox21 · Hair cell · Supporting cell

Special Issue: In Honor of Dr. Mikoshiba.

Electronic supplementary material The online version of this article (doi:10.1007/s11064-011-0416-3) contains supplementary material, which is available to authorized users.

M. Hosoya · M. Fujioka · S. Matsuda · H. Ohba · S. Shibata · F. Nakagawa · H. J. Okano · H. Okano (✉)
Department of Physiology, School of Medicine, Keio University, Tokyo, Japan
e-mail: hidokano@sc.itc.keio.ac.jp

M. Fujioka · T. Watabe · K. Wakabayashi · K. Ogawa
Department of Otolaryngology, Head and Neck Surgery, School of Medicine, Keio University, Tokyo, Japan

Y. Saga
Division of Mammalian Development and Mammalian Genetics, National Institute of Genetics, Mishima, Shizuoka, Japan

Introduction

The development of the inner ear requires a complex process of cellular morphogenesis. The first step is the specification of the otic placode in a region of ectoderm located adjacent to rhombomere 5, followed by its invagination to form the otocyst. Second, a subset of epithelial cells within the otocyst undergoes specification and develops into a sensory patch, whereas another subset delaminates and migrates to the medial and forms the cochleovestibular ganglion. Next, individual cells within the sensory patch start to differentiate into hair cells or supporting cells. This series of processes is controlled tightly and delicately by multiple molecular pathways in both a cell-intrinsic and a non-cell autonomous manner. Recently, an evolutionarily conserved transcriptional factor, Sox2, has been identified as one of the earliest markers of developing inner ear prosensory domains and had been shown to be a key player of multiple roles in cell-fate determination processes [1]. Sox2 is indeed an early permissive factor in the prosensory domain formation required for hair cell formation [1] and neuronal formation in the developing mammalian inner ear [2].

There are five Sox proteins that have been categorized as Group B Sox, which share evolutionarily conserved DNA binding domains (HMG domains) plus SoxB consensus. In contrast to the Group B1 Sox (Sox1, 2 and 3), which contain a typical activator domain at their C-terminal, Sox 14 and Sox21 are classified as Group B2 because they contain a functional repressor domain [3, 4]. Consistent with these structural biochemical characteristics, Sox1/2/3 were reported to suppress neuronal differentiation by maintaining the undifferentiated state of neural precursor cells during developmental [5–10], while Sox21 promotes neurogenesis in chicken embryonic spinal cord by counteracting Sox1/2/3 [11]. In the inner ear, the expression of Sox21 in the developing chicken has been reported, but the precise time-dependent changes that occur during development remain unknown. Here, we examined the expression profile of Sox21 at several time points using knock-in mice harboring EGFP at the Sox21 locus [12]. We found that Sox21 was expressed throughout the sensory epithelium in developing cochlea in mice. During the process of morphogenesis, Sox21 showed a unique expression pattern, and its expression was restricted in supporting cells that were in direct contact with hair cells: the inner phalangeal cells, the inner border cells, and Deiters' cells in adults. Regarding hearing functions, $Sox21^{-/-}$ mice exhibited a mild hearing impairment according to an auditory brainstem-response (ABR) analysis, together with an increase in hair cells that had lost their appropriate planar cell polarity.

Experimental Procedures

Animal

All animal care and treatment procedures were performed in accordance with institutional guidelines approved by the Experimental Animal Care Committee of the Keio University School of Medicine. Animals were housed in a room with a 12-h light/dark cycle and were fed ad libitum. *Sox21*$^{-/-}$mice were established as described previously [12] and were maintained on a C57Bl6/J background.

Immunohistochemistry

Animals were perfused with 4% paraformaldehyde (PFA; Nakalai Tesque), and the temporal bones were dissected, fixed in 4% PFA at 4°C overnight, decalcified with Decalcifying Solution. B (Wako) for 48–72 h if needed, and sliced into 6 μm sections then embedded in Tissue-Tek O.C.T. compound. The sections were preblocked for 1 h at room temperature in 10% normal serum in PBS or in 0.1% TritonX-100 (Sigma) in 10% normal serum in PBS (for anti—Myo7a and anti—NeuroD antibodies), incubated with primary antibodies at 4°C overnight, and incubated with Alexa Fluor-conjugated secondary antibodies for 60 min at room temperature. The nuclei were counterstained with Hoechst 33342. Following is the number of $Sox21^{+/EGFP}$ mice used at each stage: E10.5; $n = 3$, E16.5; $n = 3$, P0; $n = 3$, P9; $n = 3$, P14; $n = 2$, Adult; $n = 4$.

Antibodies

The primary antibodies used in this study were as follows: anti-Sox2 (goat IgG, Santa Cruz Biotechnology sc-17320, 1:100), anti-Sox21 (goat IgG, R&D AF3538, 1:100), anti-Myo7a (rabbit IgG, PROTEUS BioScience 25-6790, 1:250), anti-GFP (rabbit IgG, Medical & Biological Laboratory [MBL] 598, 1:500; goat IgG, ROCKLAND 600-101-215, 1:200), anti-NeuroD (goat IgG, santa Cruz Biotechnology sc1084, 1:100). Immunoreactivity was visualized using Alexa Fluor-conjugated secondary antibodies (Molecular Probes, 1:500). F-Actin was stained using rhodamine-phalloidin (Invitrogen R415, 1:40).

RT-PCR

The otic vesicle from E10.5 and the organ of Corti and the spiral ganglion plus Kölliker's organ from E15, P1 and P9 were dissected from wild-type C57BL/6Jcl mice under a microscope. mRNA and cDNA were prepared using an RNeasy mini kit (Qiagen) and SuperScript II (Invitrogen) according to the manufacturer's protocol. The primers for Sox21 and GAPDH were as follows, respectably: Sox21f, 5′-CACACACGTGTACATATGTA-3′; Sox21r, 5′-TCA AAACGCAACAGGTTCCG-3′; GAPDHfwd, 5′-AACGG GAAGCCCATCACC-3′; GAPDHrev, 5′-CAGCCTTGGC AGCACCAG-3′.

Whole Mount Embryo

Whole embryos of $Sox21^{+/EGFP}$ mice at E10.5 were fixed in 4% PFA and observed under a fluorescent microscope. Genotyping was confirmed retrospectively from the tail tips of each embryo as described previously [12].

Surface Preparation and Scanning Electron Microscopy (SEM)

The detailed histology of the adult organ of Corti was examined using flat-mounted surface preparations using previously reported materials and methods [13]. The prepared specimens were stained with F-actin and/or EGFP in $Sox21^{EGFP/EGFP}$, $Sox21^{+/EGFP}$ and wild-type mice ($n = 7$, 4 and 2, respectively). The ultrastructure of their surfaces

was examined using SEM in Sox21$^{EGFP/EGFP}$, Sox21$^{+/EGFP}$ and wild-type mice ($n = 2$, 3, and 3, respectively) according to a previously reported protocol [14].

Auditory Brainstem Response (ABR)

To test the auditory function of Sox21 knock-out mice, the ABR was measured in Sox21$^{EGFP/EGFP}$ and litter mate wild-type mice ($n = 4$ and 3, respectively) according to previously reported methods [15].

Results

We first performed RT-PCR for *Sox21* in the developing inner ear (Fig. 1A). *Sox21* was detected at E10.5 in the otic vesicle. At E15 and P1, *Sox21* was detected in both the organ of Corti and the Kölliker's organ. At P9, the expression in the Kölliker's organ had decreased, and no expression was detected. In contrast, the expression in the organ of Corti was maintained.

We then further analyzed the expression pattern of EGFP in Sox21$^{+/EGFP}$ mice. To confirm that the EGFP expression in the Sox21$^{+/EGFP}$ knock-in mice recapitulates the endogenous Sox21 protein expression, we double-stained for EGFP and Sox21 on cochlear cross sections of Sox21$^{+/EGFP}$ mice using anti–Sox21 and anti–GFP antibody (Supplementary Fig. S1). As shown in Fig. S1, all of the nuclei in the EGFP-positive cells were labeled with anti-Sox21 antibody, while none of the nuclei in the EGFP-negative cells were labeled. This result indicates that the EGFP expression pattern in Sox21$^{+/EGFP}$ mice reflects the endogenous protein expression of Sox21. In mouse embryos at E10.5, strong fluorescence for Sox21/EGFP was observed widely in the CNS stem cell areas. Also, EGFP was observed in the otocyst (Fig. 1B). Detailed expression in the coronal sections of the E10.5 otocyst showed that the Sox21/EGFP immunoreactivity was stronger on the ventral-lateral side, while that of Sox2 was stronger on the ventral and weaker on the dorsal side (Fig. 1C, D). The expressions of Sox2 and Sox21/EGFP were overlapped strongly on the ventral side of the otocyst, where the future cochlea was formed. In the ventral to medial region of the otic vesicle, Sox2-immunoreactivity was predominant, while Sox21/EGFP-immunoreactivity was predominant on the ventral to lateral side. At this stage, delaminated neurons from the epithelium start to form the spiral ganglion. Immunostaining showed that both EGFP and Sox2 expressions were observed in the developing spiral ganglion cells and were co-labeled with NeuroD, an early stage neuronal marker [16] (Fig. 1D-1, 2 and E-2, 3 arrows). Note that the EGFP-expression levels in the neurons were weaker than those in the future sensory epithelium region.

Cells in the organ of Corti differentiate into hair cells and supporting cells at E16.5. At E17, Sox2-expression is limited to a domain that includes both the prosensory and adjacent areas of the LER and GER [17–19]. At this stage, EGFP-immunoreactivity was widely observed in half of the cochlear duct from the apex to the base (Fig. 2A–C). Most of the Sox2-positive area was covered by a Sox21/EGFP-positive domain, both in the hair cell layer and the supporting cell layer of the sensory epithelium and GER, except in the Hensen's cells which are located in the most lateral rows of the future sensory epithelium and were positive for Sox2. Interestingly, no expression was detected in the spiral ganglion (Fig. 2A-3, B-3, arrow).

The structure of the tunnel of Corti is formed during the first two postnatal weeks in mice. At P0, Sox2-expression has been reported in a subset of differentiated supporting cells including Deiters', pillar, inner phalangeal and Hensen's cells [1]. The Sox21/EGFP-immunoreactivity was observed in Deiters' cells, pillar cells and inner phalangeal cells and Kölliker's organ (Fig. 2D, E), and the immunoreactivity in hair cells, which had been observed up to E16.5, had disappeared. No EGFP expression was observed in Sox2-positive Hensen's cells (Fig. 2E-1, arrowhead).

At P9, the tunnel of Corti had not yet been formed completely, but the developing pillar cells clearly showed their structure. At this stage, the EGFP-immunoreactivity was observed only in supporting cells, including Deiters', pillar, inner phalangeal, inner border and Hensen's cells, but the immunoreactivity in Kölliker's organ had disappeared (Fig. 3A–C). The levels of EGFP-immunoreactivity in the medial two rows of Deiters' cells, inner border cells and inner phalangeal cells were stronger, compared with the most lateral row of Deiters' cells and pillar cells. Note that the expression of Sox21/EGFP in the Sox2-positive Hensen's cells, which had not been observed at P0, had clearly re-emerged at this stage (Fig. 3B-1 arrow). Interestingly, some cells in the auditory nerve were positive for Sox21/EGFP. These cells are likely oligodendrocytes or astrocytes because the nerve fibers in the auditory nerve are axons originating from spiral ganglion neurons, of which the somas were negative for EGFP (Fig. 3A-2 arrowhead).

At P14, the structure of the organ of Corti had been almost completely formed. The Sox21/EGFP-immunoreactivity was observed in three rows of Deiters' cells, inner phalangeal cells, inner border cells and a part of Hensen's cells at this stage (Fig. 3D). The expression in the pillar cells, which were observed at P9, had disappeared, while the expression in the most lateral row of Deiters' cells was observed. The gradient of immunoreactivity for Sox21/EGFP in the Deiters' cells, which was observed at P9, was not detected at this stage.

In adults, the Sox21/EGFP-immunoreactivity was observed only in the Deiters' cells, the inner border cells,

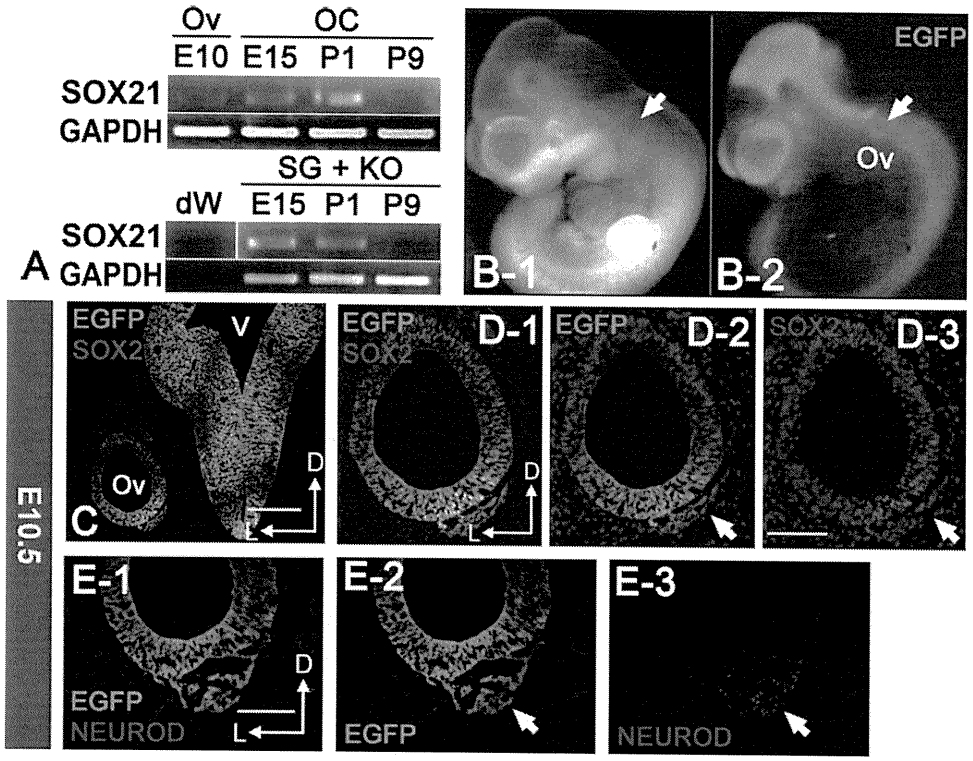

Fig. 1 Expression of Sox21 in developing inner ear. **A** RT-PCR analysis of Sox21 in wild-type mice. Sox21 was expressed in the otic vesicle at E10.5 and was detected in both the organ of Corti and the Kölliker's organ at E15 and P1, while at P9, the expression persisted only in the organ of Corti and had diminished in the spiral limbs to an undetectable level. *Ov* Otic vesicle, *OC* organ of Corti, *SG* spiral ganglion, *KO* Kölliker's organ. **B** Expression of Sox21/EGFP in E10.5 $Sox21^{+/EGFP}$ knock-in mice. At E10.5, strong EGFP-immunoreactivity was broadly observed in the CNS stem cell areas as well as the otocyst (**B-1**, **B-2** *arrows*). **C**, **D**, **E** Sox21/EGFP-expression in E10.5 inner ear. Sox21/EGFP (*green*) co-labeled with Sox2 (*red*, in **C** and **D**) and NeuroD (*red*, in **E**) in E10.5 mouse developing inner ear. In **D-2**, **3** the nuclei were counterstained with Hoechst (*blue*). Within the sensory epithelium, stronger Sox21/EGFP-expression was observed on the ventral lateral side, while for Sox2-expression, the expression was stronger on the ventral plus dorsal side. Both Sox21/EGFP and Sox2 expressions were observed in the delaminating spiral ganglion neurons (**D-2**, **D-3** *arrow*), that were colabeled with NeuroD (**E-2**, **3** *arrow*). (**C** *OV* otic vesicle, *V* fourth ventricle, Scale bar: 200 μm in **C**, 100 μm in **D**, 100 μm in **E**)

and the inner phalangeal cells. In all the rows of Deiters' cells, Sox21/EGFP-immunoreactivity was observed (Fig. 4A, B). The immunoreactivity in Hensen's cells, which were observed at P9 and P14, had disappeared.

We have already confirmed that the expression of Sox21 protein was completely abolished in homozygotes (i.e., $Sox21^{EGFP/EGFP}$) [12]. Histological analyses using a scanning electron microscope (SEM) showed that two of nine homozygote mice exhibited an increase in hair cells (Fig. 5). Interestingly, the polarity of the extra hair cells in the affected mice was disorganized, while rest of the hair cells in the same animal were normal (Fig. 5a–c). Finally, the hearing function of Sox21 knock-out mice was measured using ABR (Fig. 5d). The ABR threshold was slightly but significantly higher in the knock-out mice, compared with that in the wild-type mice, at both 8 and 16 kHz ($P < 0.05$). Thresholds of individual mice are documented in Supplementary Fig. S2.

Discussion

We showed that Sox21 was expressed in cochlear sensory epithelium throughout development but was progressively restricted to supporting cells in the mature organ of Corti: Sox21 was expressed in a broad domain containing the entirety of the future sensory epithelium at E10.5, and the expression was restricted to the inner phalangeal cells and the Deiters' cells as the inner ear matured. During this process, Sox21 showed distinctive expression patterns, as revealed by EGFP-immunoreactivity: temporally at P9, the expression level of Sox21 was not equal but exhibited a

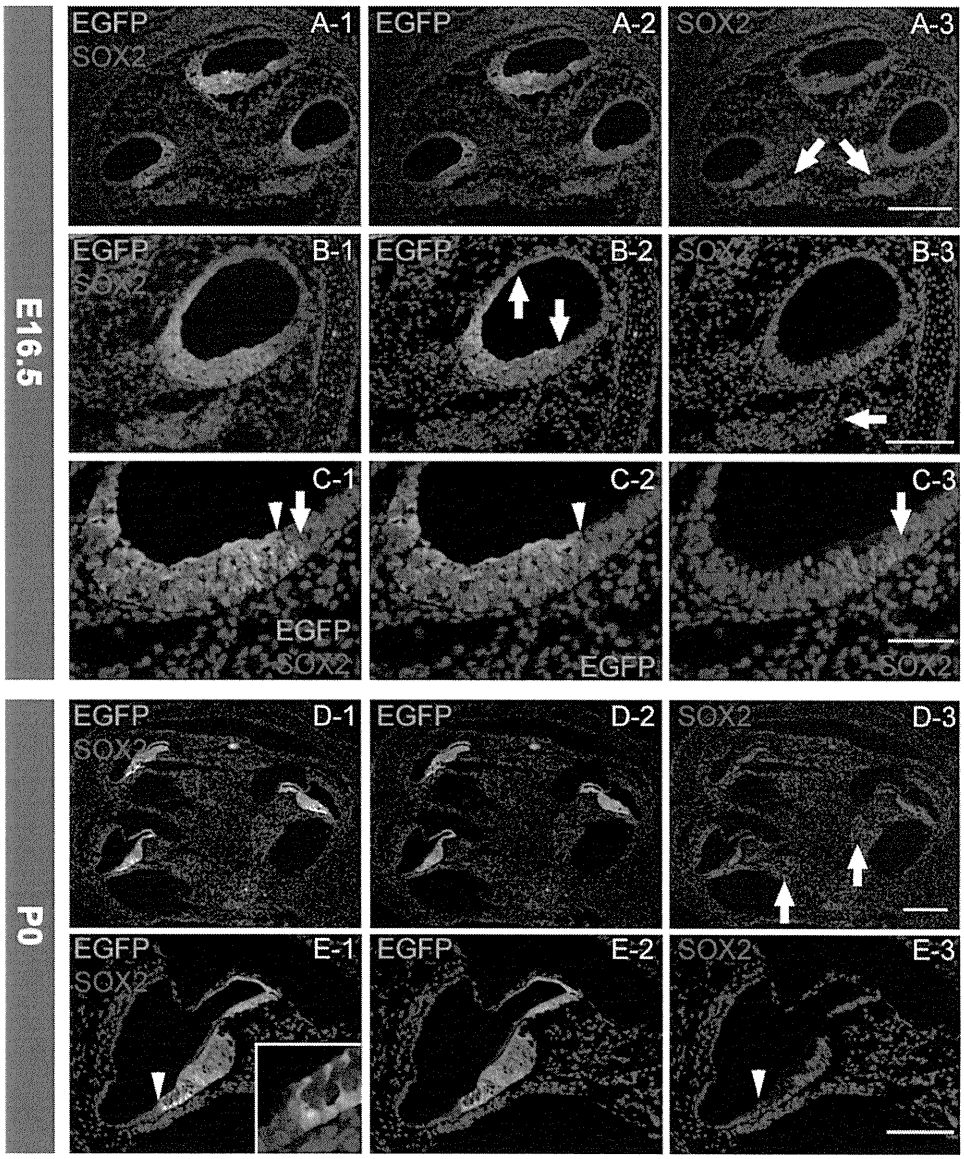

Fig. 2 Sox21/EGFP expression in the developing inner ear. **A C** Sox21/EGFP expression in E 16.5 mouse embryos. Sox21/EGFP (*green* **A-1**, **A-2**, **B-1**, **B-2**, **C-1**, and **C-2**) and Sox2 (*red* **A-1**, **A-3**, **B-1**, **B-3**, **C-1**, and **C-3**) expression patterns in E16.5 mouse developing inner ear. In each image, the nuclei were counterstained with Hoechst (*blue*). Sox21/EGFP-expression was observed only within the modiolar half of the cochlear duct (**B-2** between *arrows*), but no expression was observed in the spiral ganglion, while Sox2 expression was observed both in the future sensory epithelium and the spiral ganglion (**A-3**, **B-3** *arrow*). Note that, in the cochlea duct, the Sox21/EGFP-expression domain was wider than the region of sensory epithelium marked by Sox2 except in the Sox2-positive Hensen's cells (**C-1**, **2**, **3**; *arrow*, *arrowhead*). (Scale bar: 200 μm in **A**, 100 μm in **B**, 50 μm in **C**). **D E** Sox21/EGFP-expression in the neonate mice. Sox21/EGFP (*green* **D-1**, **D-2**, **E-1** and **E-2**) and Sox2 (*red* **D-1**, **D-2**, **E-1** and **E-3**). In each image, the nuclei were counterstained with Hoechst (*blue*). By birth, the EGFP immunoreactivity had disappeared from the hair cells, but persisted in the supporting cells except the Sox2-positive Hensen's cells (**E-1** *arrow head*). Sox21/EGFP-expression was not observed in the spiral ganglion, where Sox2 was observed. (**D-3** *arrow*) (Scale bar: 200 μm in **D**, 100 μm in **E**)

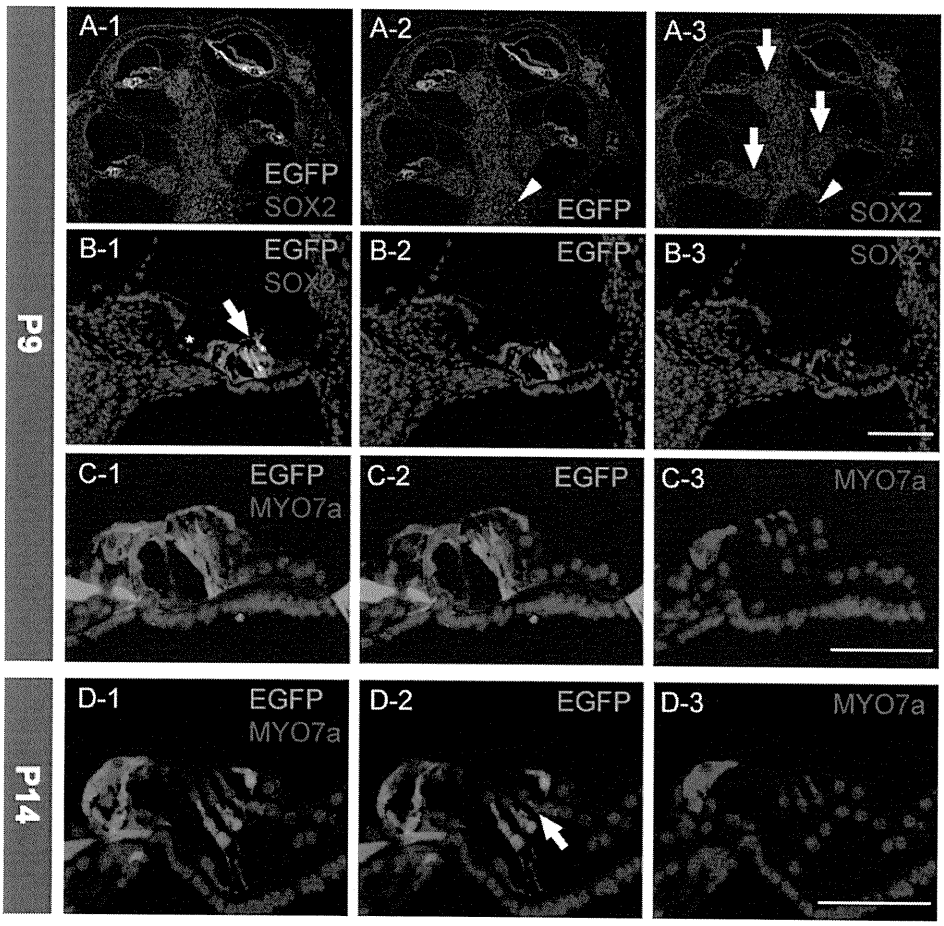

Fig. 3 Expression of Sox21/EGFP in the postnatal cochlea. **A C** Sox21/EGFP-expression at P9. Sox21/EGFP (*green* **A-1**, **A-2**, **B-1**, **B-2**, **C-1** and **C-2**), Sox2 (*red* **A-1**, **A-3**, **B-1** and **B-3**) and Myosin 7a (*red* **C-1** and **C-3**). In each image, the nuclei were counterstained with Hoechst (*blue*). Sox21/EGFP expression was not observed in the spiral ganglion, while Sox2 expression was consistently observed (**A-3** *arrow*). EGFP-expression was observed in the inner phalangeal cells, medial two rows of Deiters' cells, inner border cells, pillar cells and Sox2-positive Hensen's cell (**B-1** *arrow*). Some cells in the central portion of auditory nerve were positive for both Sox21/EGFP and Sox2, most likely oligodendrocytes or astrocytes. (**A-2** and **A-3** *arrowhead*) (**B**) Sox21/EGFP expression was not observed in hair cells (**C**) and the GER or spiral limbs (**B-1** *asterisk*). The expression of Sox21/EGFP in Deiters' cells, inner border cells and inner phalangeal cells was strong, but was relatively weak in the most lateral row of Deiters' cells and the pillar cells. (**B-2**, **C-2**) (Scale bar: 200 μm in **A**, 100 μm in **B**, 50 μm in **C**). **D** Sox21/EGFP expression in P14 organ of Corti. Sox21/EGFP (*green* **D-1** and **D-2**) and Myosin 7a (*red* **D-1** and **D-3**). In each image, the nuclei were counterstained with Hoechst (*blue*). EGFP-expression was observed only in the inner phalangeal cells, inner border cells, three rows of Deiters' cells and part of Hensen's cell. **D** EGFP expression was observed in the most lateral row of Deiters' cells. No apparent gradient of expression was observed among the Deiters' cells (**D-2** *arrow*). In the pillar cells, EGFP expression was diminished and no longer observed, while it was observed at P9. (Scale bar: 50 μm in **D**)

gradient among the three rows of the Deiters' cells, with high expression in the modiolar two rows and low expression in the lateral row (Fig. 4C). The expression once again became homogenous at P14. This phenomenon was accompanied by the temporal expression of EGFP in the Hensen's cells between P9 and P14, which did not become positive until P0 and after P28. These findings may indicate that the three rows of Deiters' cells are not the same with respect to their characteristics as potential progenitor cells, at least during the development process, leading us to speculate that Sox21 might be involved in the delicate spatiotemporal maturation of individual supporting cells.

The physiological function of Sox21 appears to depend on the cellular context in a neuronal cell line [11, 20].

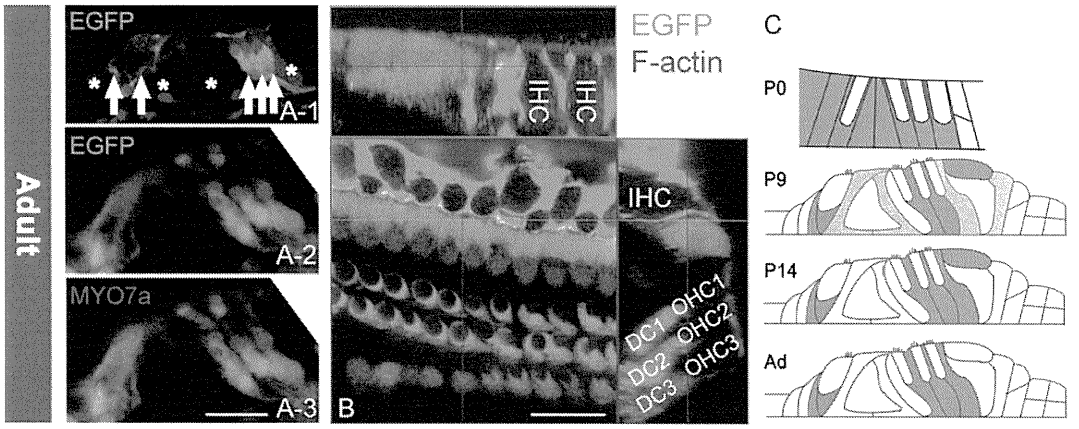

Fig. 4 Sox21/EGFP expression in adult. **A** **B** Sox21/EGFP expression in adult organ of Corti. Sox21/EGFP (*green* **A-1**, **A-2**, **A-3** and **B**), Myosin 7a (*red* **A-3**) and F-actin (*red* **B**). The nuclei were counterstained with Hoechst (*blue*). In the adult (4 weeks old) cochlea, EGFP-immunoreactivity was observed only in supporting cells that directly contacted with the hair cells: Deiter' s cell, inner border cells and inner phalangeal (**A-1** *arrows*). Note that no expression was observed in hair cells, pillar cells, Hensen's cells (**A-1** *asterisks*). (Scale bar: 25 μm in **A**, 25 μm in **B**). **C** Schema of Sox21/EGFP-expression pattern in the developing cochlea. Summary of the distinctive expression patterns of Sox21 in the developing organ of Corti. At P0, EGFP expression was observed in supporting cells except Sox2-positive Hensen's cells and the modiolar half of the cochlear duct. No immunoreactivity was observed in the hair cells. At P9, EGFP expression was observed only in supporting cells. The immunoreactivity observed in the inner phalangeal cells, inner border cells, medial two rows of Deiters' cells, and part of the Hensen's cells was strong, while the immunoreactivity observed in the most lateral Deiters' cells and pillar cells was relatively weak. At P14, the expression was observed in inner phalangeal cells, inner border cells, three rows of Deiters' cells, and part of the Hensen's cells. In adults, the expression was observed only in the inner phalangeal cells, inner border cells, and Deiters' cells (Ad: Adult)

Notably, in the skin, we found that Sox21 is required for the fine-tuned differentiation of hair shafts and is required for the formation of the cuticle, which is essential for the solid junction of hairs and follicles of the skin [12]. During the development of the inner ear, previous reports have revealed that Sox2 is required for the prosensory domain formation of the cochlea: mouse mutants with no or reduced expression of Sox2 in the developing inner ear develop a severe inner ear malformation with no or a reduced number of hair cells [17]. Previous reports have revealed that Sox21 is the only Group B2 Sox expressed in the cochlea throughout development [3, 4]. Here, we found that the distinctive spatiotemporal changes of Sox21 expression in the developing cochlea partially overlapped with those of the Group B1 Sox family, including Sox2. Although the role of Sox21 in the developing and adult inner ear remains to be elucidated, Sox21 may counteract Sox2 in developing prosensory cells to control the fine-tuned formation of hair cells. In addition, Sox21 might also be responsible for the differentiation of particular subsets of supporting cells, such as Deiter's and phalangeal cells, as is also the case with hair shaft differentiation in the skin. Further analyses of Sox21 mutant mice should help to solve this question.

At E10.5, Sox21 was expressed in the developing spiral ganglion, but no expression was observed after E16, in contrast to the expression of Sox2 observed throughout the process of developing cochleovestibular neurons, as previously reported [19]. In addition, Sox2 was also known to induce neuronal formation in the developing mammalian cochlea [2]. Our findings suggest that, unlike developing spinal cord [11], the differentiation of the cochleovestibular ganglion might not be dependent on Sox21.

The phenotypes of homozygote Sox21 knock-in and knock-out mice seem intriguing. The increase in hair cells was severer for the outer hair cells and lesser for the inner hair cells, similar to observations in Hes5 knock-out mice [21]. Although the penetrance of the phenotype was approximately 20%, the data suggests that sensory epithelium formation might possibly be mediated by Notch-related genes, such as Hes5. Further study to understand the role of Sox21 in both hair cells and subsets of supporting cells should be attempted, particularly the downstream target genes of Sox21.

Previous studies have shown that supernumerous hair cells lead to severe hearing loss; for instance, in pRb conditional knock-out mice, the hearing threshold was severely affected by 40 dB as a result of the delayed cell death, while each hair cell had a functional mechano-transduction channel [22]. In contrast, in Sox21 knock-out mice, the hearing impairment was as slight as 10 dB; an increase in hair cells was observed, but the increase was

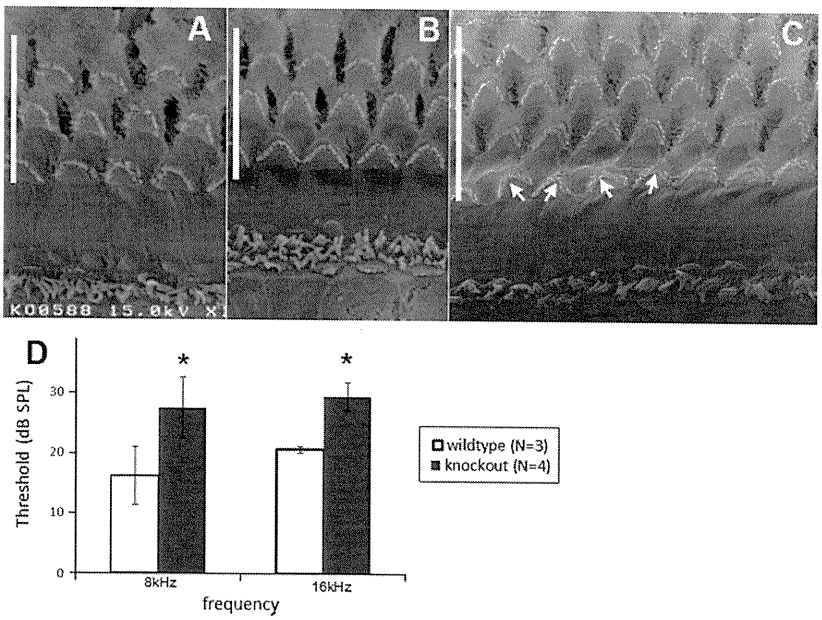

Fig. 5 Phenotype of Sox21$^{EGFP/EGFP}$ or Sox21 knock-out mice in adults. **a** c Extra hair cells in Sox21 $^{-/-}$ missing planar cellular polarity. Scanned electron microscopy images of wild-type, Sox21$^{+/-}$ and Sox21 $^{-/-}$ mice (**a**, **b** and c, respectively). In the knock-out mice, supernumerary outer hair cells (*OHCs*) were observed from the basal to apical turns. The first row of OHCs missed their polarities (*arrows*), while the others seemed normal (c). **d** Slight but significant impairment of hearing in Sox21 knock-out mice. An auditory brainstem response (*ABR*) analysis was performed in Sox21 $^{-/-}$ mice and litter mate wild-type mice ($n = 4$ and 3, respectively) at 8 and 16 kHz. The hearing threshold was significantly elevated in the knock-out mice, compared with the wild-type mice, but only by 10 dB at both frequencies ($^*P < 0.05$, Mann Whitney U test)

not as severe as that in the pRB conditional knock-out mice and the structure of the organ of Corti—one layer of hair cells lying over a layer of supporting cells—was completely preserved. Our findings do not lead to the conclusion that the hearing impairment was due to the increase in hair cells because Sox21 expression was observed not only in the supporting cells, but also in the auditory nerve, most likely in oligodendrocytes or astrocytes. However, these results suggest that not only a sufficient number, but also an appropriate physiological structure for the hair cells is required for the function of the organ of Corti. Regaining a suitable number of hair cells at the correct position or on the supporting cells may be important for a functional outcome in regenerative medicine for patients with hearing loss.

Unlike some supporting cell markers including GFAP [23], S100A1 [24], Prox1 [25], TC2 [26], p75^{NTR} [27], Jagged1 [28], GLAST [29] and Sox2 [18, 19], Sox21 expression persists into adulthood, especially in Deiters' cells, inner border cells and phalangeal cells. Supporting cells in the organ of Corti include several distinct subpopulations that are morphologically different, yet only three types of cells are in direct contact with the hair cells: the inner phalangeal cells, the inner border cells, and Deiters' cells. Our results clearly demonstrated that Sox21 expression was observed only in the supporting cells that are in direct contact with the hair cells in adult cochlea. This finding shows that Sox21 is a novel marker of supporting cells neighboring hair cells. Moreover, the results suggest that genetic modification using the Sox21 locus, such as Cre knock-in, may be a useful tool for targeting supporting cells that are in direct contact with hair cells, including specific gene expression. Furthermore, gene delivery or therapy using a Sox21 enhancer or promoter may have feasible clinical applications, particularly for inducing hair cells at the proper positions, as discussed previously.

In conclusion, we showed that Sox21 is expressed in developing and adult cochlea. A broad expression of Sox21, including the otocyst and delaminating neurons, became restricted to supporting cells, and finally was only expressed in cells in direct contact with hair cells. Since the expression pattern was extremely distinctive, this pattern may be useful for labeling a subset of supporting cells in detailed analyses of the organ of Corti. Furthermore, our findings in Sox21 knock-out mice indicate that Sox21 plays

an important role in the development and in the physiological function of the cochlea. Further analyses examining the function of this intriguing repressor Sox B protein in supporting and hair cell differentiation are awaited in the near future.

Acknowledgments We thank Ms. Ayano Mitsui and Dr. T. Nagai for their technical assistance and Dr. Junko Murata (Osaka University) for technical advices. This work was supported by grants from the Ministry of Education, Culture, Sports, Science and Technology (MEXT), the Japan Science and Technology Corporation (JST), and the Funding Program for World-leading Innovative R&D on Science and Technology to H.O., and by a Grant-in-Aid for Scientific Research B (20390444) to K.O., and by a Research on Measures for Intractable Diseases from the Ministry of Health, Labor and Welfare of Japan to M.F., and by a Keio University grant-in-aid for encouragement of young medical scientists to M.F., and by a Keio Gijuku Academic Development Funds to M.F. and by a Grant-in-Aid for Young Scientists B (22791628) to M.F. from MEXT. and by a grant-in-aid from the Global COE Program of MEXT, Japan to Keio University.

References

1. Dabdoub A, Puligilla C, Jones JM et al (2008) Sox2 signaling in prosensory domain specification and subsequent hair cell differentiation in the developing cochlea. Proc Natl Acad Sci USA 105:18396–18401
2. Puligilla C, Dabdoub A, Brenowitz SD et al (2010) Sox2 induces neuronal formation in the developing mammalian cochlea. J Neurosci 30:714–722
3. Uchikawa M, Kamachi Y, Kondoh H (1999) Two distinct subgroups of Group B Sox genes for transcriptional activators and repressors: their expression during embryonic organogenesis of the chicken. Mech Dev 84:103–120
4. Bowles J, Schepers G, Koopman P (2000) Phylogeny of the SOX family of developmental transcription factors based on sequence and structural indicators. Dev Biol 227:239–255
5. Bani-Yaghoub M, Tremblay RG, Lei JX et al (2006) Role of Sox2 in the development of the mouse neocortex. Dev Biol 295:52–66
6. Bylund M, Andersson E, Novitch BG et al (2003) Vertebrate neurogenesis is counteracted by Sox1-3 activity. Nat Neurosci 6:1162–1168
7. Favaro R, Valotta M, Ferri AL et al (2009) Hippocampal development and neural stem cell maintenance require Sox2-dependent regulation of Shh. Nat Neurosci 12:1248–1256
8. Ferri AL, Cavallaro M, Braida D et al (2004) Sox2 deficiency causes neurodegeneration and impaired neurogenesis in the adult mouse brain. Development 131:3805–3819
9. Kan L, Israsena N, Zhang Z et al (2004) Sox1 acts through multiple independent pathways to promote neurogenesis. Dev Biol 269:580–594
10. Wang TW, Stromberg GP, Whitney JT et al (2006) Sox3 expression identifies neural progenitors in persistent neonatal and adult mouse forebrain germinative zones. J Comp Neurol 497: 88–100
11. Sandberg M, Kallstrom M, Muhr J (2005) Sox21 promotes the progression of vertebrate neurogenesis. Nat Neurosci 8:995–1001
12. Kiso M, Tanaka S, Saba R et al (2009) The disruption of Sox21-mediated hair shaft cuticle differentiation causes cyclic alopecia in mice. Proc Natl Acad Sci USA 106:9292–9297
13. Masuda M, Nagashima R, Kanzaki S et al (2006) Nuclear factor-kappa B nuclear translocation in the cochlea of mice following acoustic overstimulation. Brain Res 1068:237–247
14. Mizutari K, Fujioka M, Nakagawa S et al (2010) Balance dysfunction resulting from acute inner ear energy failure is caused primarily by vestibular hair cell damage. J Neurosci Res 88:1262–1272
15. Fujioka M, Kanzaki S, Okano HJ et al (2006) Proinflammatory cytokines expression in noise-induced damaged cochlea. J Neurosci Res 83:575–583
16. Lawoko-Kerali G, Rivolta MN, Lawlor P et al (2004) GATA3 and NeuroD distinguish auditory and vestibular neurons during development of the mammalian inner ear. Mech Dev 121: 287–299
17. Kiernan AE, Pelling AL, Leung KK et al (2005) Sox2 is required for sensory organ development in the mammalian inner ear. Nature 434:1031–1035
18. Hume CR, Bratt DL, Oesterle EC (2007) Expression of LHX3 and SOX2 during mouse inner ear development. Gene Expr Patterns 7:798–807
19. Mak AC, Szeto IY, Fritzsch B et al (2009) Differential and overlapping expression pattern of SOX2 and SOX9 in inner ear development. Gene Expr Patterns 9:444–453
20. Ohba H, Chiyoda T, Endo E et al (2004) Sox21 is a repressor of neuronal differentiation and is antagonized by YB-1. Neurosci Lett 358:157–160
21. Zine A, Aubert A, Qiu J et al (2001) Hes1 and Hes5 activities are required for the normal development of the hair cells in the mammalian inner ear. J Neurosci 21:4712–4720
22. Sage C, Huang M, Vollrath MA et al (2006) Essential role of retinoblastoma protein in mammalian hair cell development and hearing. Proc Natl Acad Sci USA 103:7345–7350
23. Rio C, Dikkes P, Liberman MC et al (2002) Glial fibrillary acidic protein expression and promoter activity in the inner ear of developing and adult mice. J Comp Neurol 442:156–162
24. Coppens AG, Kiss R, Heizmann CW et al (2001) Immunolocalization of the calcium binding S100A1, S100A5 and S100A6 proteins in the dog cochlea during postnatal development. Brain Res Dev Brain Res 126:191–199
25. Bermingham-McDonogh O, Oesterle EC, Stone JS et al (2006) Expression of Prox1 during mouse cochlear development. J Comp Neurol 496:172–186
26. Bianchi LM, Liu H, Krug EL et al (1999) Selective and transient expression of a native chondroitin sulfate epitope in Deiters' cells, pillar cells, and the developing tectorial membrane. Anat Rec 256:64–71
27. Sato T, Doi K, Taniguchi M et al (2006) Progressive hearing loss in mice carrying a mutation in the p75 gene. Brain Res 1091: 224–234
28. Murata J, Tokunaga A, Okano H et al (2006) Mapping of notch activation during cochlear development in mice: implications for determination of prosensory domain and cell fate diversification. J Comp Neurol 497:502–518
29. Jin ZH, Kikuchi T, Tanaka K et al (2003) Expression of glutamate transporter GLAST in the developing mouse cochlea. Tohoku J Exp Med 200:137–144

Eur Arch Otorhinolaryngol (2011) 268:973–978
DOI 10.1007/s00405-011-1484-3

OTOLOGY

Acoustic overstimulation-induced apoptosis in fibrocytes of the cochlear spiral limbus of mice

Yong Cui · Guang-wei Sun · Daisuke Yamashita · Sho Kanzaki · Tatsuo Matsunaga · Masato Fujii · Kimitaka Kaga · Kaoru Ogawa

Received: 10 July 2010 / Accepted: 6 January 2011 / Published online: 19 January 2011

Abstract Fibrocytes of the spiral limbus are thought to play a significant role in maintaining ion homeostasis in the cochlea. The present study measured physiological and morphological changes in spiral limbus of mice in response to noise exposure. 6-week-old male C3H/HeJJcl mice were exposed to octave-band noise (120 dB SPL) for 2 h and evaluated at a series of times thereafter, up to 8 weeks. Permanent hearing loss resulted in the mice, as assessed by auditory brainstem response (ABR) recordings. The fibrocytes loss was found in the spiral limbus of the apical turn, which has been proved to be induced by apoptosis. These results suggest that noise exposure might result in apoptosis of fibrocytes in spiral limbus, which suggest a mechanism for noise-induced hearing loss.

Keywords Spiral limbus · Fibrocytes · Noise · Hearing loss

Yong Cui and Guang-wei Sun equally contributed to this work.

Y. Cui · D. Yamashita · S. Kanzaki · K. Ogawa
Department of Otolaryngology,
School of Medicine, Keio University,
35 Shinanomachi, Shinjuku-ku,
Tokyo 160-8582, Japan

Y. Cui · G. Sun · D. Yamashita · T. Matsunaga · M. Fujii · K. Kaga
Laboratory of Auditory Disorders,
Division of Hearing and Balance Research,
National Institute of Sensory Organs,
National Tokyo Medical Center,
2-5-1 Higashigaoka, Meguro-ku,
Tokyo 152-8902, Japan

Y. Cui
Department of Otolaryngology,
Guangdong Academy of Medical Sciences
& Guangdong General Hospital,
106 Zhongshan Second Road,
Guangzhou 510080, People's Republic of China

G. Sun (✉)
Lab of Biomedical Material Engineering,
Dalian Institute of Chemical Physics,
The Chinese Academy of Sciences,
457 Zhongshan Rd, Dalian 116023, China
e-mail: sunrise124@gmail.com

Introduction

Histopathology associated with noise-induced hearing loss has been studied extensively and most of the research generally focused on pathological alterations in the hair cells and stereocilia [1–3]. The damage to other sensory structures, for example, afferent dendrites, and spiral ganglion cells (SGCs) can also lead to hearing loss [4, 5].

The functions of hair cells depend on the ionic homeostasis (especially K^+) in the endolymph, which is maintained by the K^+ recycling in the inner ear. The lateral wall and spiral limbus in the cochlea play an important role in the K^+ recycling, which can transport the K^+ ions actively by ion-exchange enzyme systems [6].

Hirose and colleagues [1, 7] characterized noise injury extending beyond the sensory structures to non-sensory structures (strial vascularis, spiral ligament and spiral limbus). In mice and other models, the morphological, enzymatic, and cytochemical features of the lateral wall, especially the stria, changed markedly hours and days after noise exposure [8–10].

Although the pathological change in the spiral limbus has been reported previously [1, 11–13], the time course of those morphological changes and the mechanism under them have not been well studied. In the present study, we tried to answer those questions.

Materials and methods

Animals and experimental groups

Male C3H/HeJJcl mice aged 6 weeks were used in the present study. Previous study showed that C3H mouse maintained excellent cochlear function throughout the first year of his age [14]. Animals were randomly assigned to serve as control or as noise-exposed subjects. The experimental groups included the following nine groups of mice ($n = 3$ per group) that were assessed 0, 6, 12, 24 h, 3 days, 1, 2, 4 and 8 weeks, respectively, after noise exposure. All mice underwent auditory brainstem response (ABR) threshold testing before being exposed to noise and immediately prior to killing. All experiments were conducted in accordance with the guidelines of the National Institutes of Health and the Declaration of Helsinki, and guidelines set by the Keio University Union on Laboratory Animal Medicine.

Noise exposure

Mice from each experimental group were placed in a custom-made sound chamber fixed within individual compartments of a metallic mesh cage which can hold four animals. The sound chamber was fitted with a speaker driven by a noise generator (AA-67N; RION Co., Ltd., Tokyo, Japan) and two power amplifiers (SRP-P150; Sony, Tokyo, Japan, and D-1405; Fostex, Chesterfield, MO). In all the experimental groups, the animals were exposed to one octave-band noise centered at 4 kHz, at 120 dB SPL for 2 h. Sound levels were calibrated and measured with a sound level meter (NL-20; RION Co., Ltd., Tokyo, Japan) placed at the level of the animal's head.

Auditory brainstem response (ABR) recordings

Auditory brainstem responses were evoked as described previously [15]. ABR recordings were performed with an extracellular amplifier Digital Bioamp system (BAL-1; Tucker-Davis Technologies, Alachua, FL), and waveform storing and stimulus control were performed with PowerLab systems Scope software (PowerLab 2/20; ADInstruments, Castle Hill, Australia). Sound stimuli were produced with a coupler type speaker (ES1spc; Bioresearch Center, Nagoya, Japan), which was inserted into the external auditory canal of each mouse. Mice were anesthetized with ketamine (80 mg/kg, i.p.) and xylazine (15 mg/kg, i.p.), and then implanted with stainless steel needle electrodes, which were placed at the vertex and ventrolateral to the left and right ears. Tone burst stimuli (0.1 ms rise/fall time; 1 ms flat segment) were used as test tones. Generally, the ABR waveforms were recorded for 12.8 ms at a sampling rate of 40,000 Hz using 50–5,000 Hz band-pass filter settings; waveforms from 1,024 stimuli at a frequency of 9 Hz were averaged. The ABR waveforms were recorded at 5 dB SPL intervals. The stimulus threshold was defined as the lowest sound level at which a recognizable waveform could still be seen. Because the sound level of test tones generated from the machine is limited, we set the stimulus threshold to 89.7, 91.7, and 83.2 dB SPL at 4, 8, and 16 kHz, respectively, when a mouse failed to respond due to profound noise-induced hearing impairment. The left and right ears of each mouse were used for ABR recording.

Histological preparations

After anesthetization with xylazine (15 mg/kg, i.p.) and ketamine (80 mg/kg), the animals were perfused transcardially with cold 0.01 M phosphate-buffered saline (PBS; pH 7.4), followed by 4% paraformaldehyde in 0.1 M PB. The left cochleas were extracted ($n = 3$, each time point), and a hole was made in the apex to allow intra-labyrinthine perfusion with the fixative. After overnight post-fixation in the same fixative at 4°C, cochleas were decalcified with buffered 0.1 M ethylenediaminetetraacetate (EDTA, pH 7.5) for 1 week at 4°C. Cochleas were dehydrated through a graded ethanol series and xylene, embedded in paraffin, and then sectioned in the midmodiolar plane at 5.0 μm. Light microscope: the slides containing cochlea sections were stained with hematoxylin and eosin (H&E) (Sakura Finetek Japan, Tokyo, Japan) to view the structure. The specimens were viewed with a laboratory microscope (DM 2500; Leica, Houston, TX). In the present study, the cochlea was divided into four half turns (lower basal, upper basal, lower apical, and upper apical). The fibrocytes in the spiral limbus of the lower apical turn were counted.

The cell density calculation was performed as described previously [16]. The cell density of fibrocytes in the spiral limbus, lateral wall and SGCs within the lower apical turn was calculated after H&E staining ($n = 15$, each time point). Area measurement and cell count were performed using ImageJ, a java-based image analysis program developed at the US National Institutes of Health.

Apoptosis detection

The TUNEL assay was performed with an apoptosis in situ detection kit (Wako, Osaka, Japan) according to the manufacturer's instructions ($n = 3$, each group). Negative controls were subjected to proteinase K digestion but not terminal deoxynucleotidyl transferase (TdT) treatment. Distilled water was substituted for TdT reagent in the negative controls.

The detection of anti-single-stranded DNA (ssDNA) was done as follows: after deparaffinization, the sections were